Covalent Triazine Frameworks-derived N,P Dual-doped Porous Carbons for Highly Efficient Electrochemical Reduction of $CO_2$①

ZHANG Meng-Di[a, b, d] YI Jun-Dong[b, c]
HUANG Yuan-Biao[b, c, d②] CAO Rong[b, c, d②]

[a] (*College of Chemistry and Materials Science, Fujian Normal University, Fuzhou* 350007, *China*)
[b] (*State Key Laboratory of Structural Chemistry, Fujian Institute of Research on the Structure of Matter, Chinese Academy of Sciences, Fuzhou* 350002, *China*)
[c] (*University of Chinese Academy of Sciences, Beijing* 100049, *China*)
[d] (*Fujian College, University of Chinese Academy of Sciences, Fuzhou* 350002, *China*)

ABSTRACT Electroreduction of CO_2 into chemicals is of great importance in the global carbon balance. Although noble-metal based catalysts and single-atom catalysts (SACs) are known to be active for CO_2 electroreduction reaction (CO_2RR), the high cost of noble-metal and the lack of effective synthesis approaches to prepare SACs have tremendously hindered the application. Non-metal doped carbon materials have attracted great interest because of their reasonable cost, chemical stability and excellent electrical conductivity. Nevertheless, the design and fabrication of highly efficient non-metal doped carbon electrocatalysts for CO_2RR to meet industry demands still remains a big challenge. Herein, triphenylphosphine@covalent triazine framework~~s~~ (CTF~~s~~) composite~~s~~ were employed as precursors to fabricate N,P dual-doped porous carbon catalysts PCTF-X-Y (X represents the carbonization temperature, and Y represents the mass ratio of CTF to triphenylphosphine) for CO_2RR. Due to the high specific surface areas and synergistic effect between N and P, the obtained PCTF-1000-5 exhibited high selectivity for CO production up to 84.3% at –0.7 V versus the reversible hydrogen electrode (vs. RHE) and long-term durability over 16 h, which are better than the reported N,P dual-doped carbon catalysts in aqueous media. This work provides a new way to design and fabricate non-metal catalysts for electrocatalysis.

Keywords: carbon dioxide, electrocatalysis, covalent triazine frameworks, N,P dual-doped carbons, carbon monoxide; DOI: 10.14102/j.cnki.0254–5861.2011–3118

1 INTRODUCTION

The electroreduction of CO_2 into value-added chemicals using renewable electricity would be a promising way to alleviate the greenhouse effect and achieve a neutral carbon cycle[1-9]. Among the products of CO_2 electroreduction reaction (CO_2RR), CO is considered to be one of the most important industrial feedstocks, which has been widely used for the Fischer-Tropsch synthesis to produce hydrocarbon liquid fuels[10-13]. In the past decades, noble-metal (e.g., Au, Ag, and Pd) based catalysts and single-atom catalysts (SACs) (e.g., Ni–N–C and Co–N–C) have been successfully developed and widely used as highly active electrocatalysts for CO_2RR to produce CO[14-23]. Nevertheless, the applications of noble-metal based catalysts are limited by their exorbitant prices, while in the case of SACs, it is difficult to fabricate SACs in large-scale manner with simple synthesis procedures[24-27]. Therefore, it is an urgent desire to develop efficient metal-free electrocatalysts such as non-metal doped carbon materials towards CO_2RR. Recently, the metal-free porous carbons have drawn considerable attention because of their intrinsic features of low-cost, earth abundance, large surface area, excellent conductivity and stability in acidic and alkaline media in comparison to the

Received 5 January 2021; accepted 3 March 2021

① Financial support from the National Key Research and Development Program of China (2018YFA0208600, 2018YFA0704502), NSFC (21871263, 22071245, 22033008), Strategic Priority Research Program of the Chinese Academy of Sciences (XDB20000000) and the Youth Innovation Promotion Association, CAS (Y201850)

② Corresponding authors. Tel: 13599056269. E-mails: ybhuang@fjirsm.ac.cn (Y.-B. Huang) and rcao@fjirsm.ac.cn (R. Cao)

metal-based electrocatalysts[28-31]. A variety of non-metal atoms (e.g., N, P, F, etc.) doped carbons are active in CO_2RR for the production of CO[32-34]. The high CO_2RR activity for these carbons is attributed to that the introduction of foreign atoms into the carbon skeleton could break the electroneutrality of carbon matrix and induce the charged active sites[1, 29, 30, 35]. Compared with the single non-metal atom doping, dual-doped carbons usually achieve higher electrocatalytic activity owing to the increase of activated centers and the synergistic effect between the different dopants[30, 35]. Unfortunately, it still remains a significant challenge for the heteroatom doped carbons to achieve highly efficient CO_2RR due to the lack of enough active sites to overcome the inert chemical bond of CO_2 molecules and the competitive side reactions such as the hydrogen evolution reaction (HER).

As a common heteroatom, nitrogen (N) has been widely employed as dopant incorporated into carbon matrix[1, 29, 30, 32, 35-37] and the resulting N-doped carbons exhibited enhanced electrocatalytic activity due to the higher electronegativity of N with respect to C and the formation of positive charge density on the adjacent C[1, 29, 30, 35]. Unlike N, phosphorus (P) with lower electronegativity than C can modify the local charge of N-doped carbons to obtain an optimized charge-carrier concentration and create new active sites[30, 35, 38], which are considered as an ideal dopant together with N atom for the fabrication of dual-doped carbons. Regarding ORR, it has been demonstrated that the N and P dual-doped carbon materials present high activity and durability[39, 40]. Nevertheless, the CO_2RR catalyzed by N,P dual-doped carbon materials has seldom been investigated[40, 41].

Covalent triazine frameworks (CTFs) constructed from the trimerization of aromatic nitriles are one class of porous conjugated polymers containing high N content[42-45], which have been identified as ideal precursors to prepare highly porous carbons[46]. Moreover, the highly porous structures in CTFs are beneficial for the introduction of triphenylphosphine (PPh_3) into the pores as P source. In addition, the superior chemical and thermal stability of CTFs is beneficial to obtain high carbon yield.

In this work, PPh_3 as phosphorus source was encapsulated into the pores of CTF-400 (Fig. 1), which was employed as precursors to fabricate N,P dual-doped porous carbons PCTF-X-Y, where X represents the carbonization temperature and Y is the mass ratio of CTF to PPh_3. The N and P contents in the obtained materials can be adjusted by changing the mass ratio between CTF-400 and PPh_3 as well as the carbonization temperature. Due to the high specific surface areas and the synergistic effect caused by the doped N and P in the graphitic networks, the resulting PCTF-1000-5 catalyst exhibited high CO selectivity with 84.3% faradaic efficiency (FE) at –0.7 V versus the reversible hydrogen electrode (vs. RHE, all potentials are with reference to the RHE), which is 1.5 times higher than that of mono N-doped CTF-1000 at the same potential. As far as we know, the high CO selectivity outperforms all previously reported N,P dual-doped CO_2RR electrocatalysts in aqueous system[40] and most of metal-free carbons[12, 32-34, 37, 40, 41, 47-53]. Moreover, PCTF-1000-5 could maintain its initial activity over 16 h during the long-term electrolysis experiment.

2 RESULTS AND DISCUSSION

The preparation of N,P dual-doped porous carbons is illustrated in Fig. 1. Typically, the porous covalent triazine framework, CTF-400, acted as nitrogen source and precursor was prepared from the trimerization of terephthalonitrile in the presence of molten $ZnCl_2$ as Lewis catalyst and porogen[42, 46]. As measured by the inductively coupled plasma atomic emission spectrometry (ICP-AES), the content of Zn in CTF-400 is less than 0.23 wt%, suggesting that the residual $ZnCl_2$ has been removed using diluted hydrochloric acid. The PPh_3 was introduced into CTF-400 by a facile impregnation method, followed by carbonization to give N,P dual-doped porous carbons PCTF-X-Y (X = 600 ℃, 800 ℃ and 1000 ℃; Y = 5 and 1). When the mass ratios of CTF-400 to PPh_3 are 5:1 and 1:1 (carbonization temperature is 1000 ℃), the corresponding samples were named as PCTF-1000-5 and PCTF-1000-1. For comparison, the N-doped carbon CTF-1000 was obtained by pyrolysis of CTF-400 at 1000 ℃. The samples carbonized at different temperature of 600, 800 and 1000 ℃ (the mass ratio of CTF-400 to PPh_3 is 5:1) were denoted as PCTF-600-5, PCTF-800-5 and PCTF-1000-5, respectively. For N,P dual-doped carbon materials and CTF-1000, the N and P contents are summarized in Table S1 based on the elemental analysis (EA) and ICP-AES results. It can be observed that the contents of N and P in PCTF-1000-5 are 1.99 wt% and 0.46 wt%, respectively. The N and P contents decreased as the mass ratio of CTF-400 and PPh_3 decreased at the same carbonization temperature, while with decreasing the carbonization temperature, the N and P contents increased under the same mass ratio between CTF-400 and PPh_3.

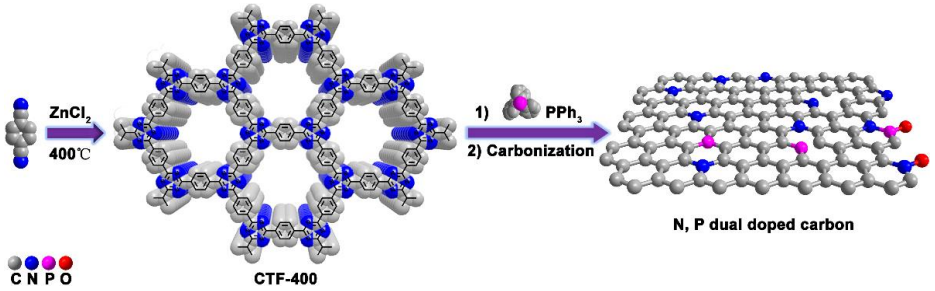

Fig. 1. Schematic illustration for the synthesis of CTF-400 and N,P dual-doped porous carbons from PPh_3@CTF-400. Hydrogen atoms are omitted for simplicity

The powder X-ray diffraction (PXRD) patterns of CTF-400 (Fig. S1) shows only an obvious broad peak at around 25 °indexed to the (001) reflection of aromatic sheets. The N_2 adsorption-desorption measurement of precursor CTF-400 was performed at 77 K (Fig. S2), which revealed that CTF-400 has a high Brunauer-Emmett-Teller (BET) surface area of 568 $m^2 g^{-1}$ and a large total pore volume of 0.32 $cm^3 g^{-1}$. The pore size distribution determined by the nonlocal density functional theory (NL-DFT) method (Fig. S2) revealed that the CTF-400 is mainly composed with micropores. The micropore of 1.2 nm matches well with the pore size of 11.55 Å measured from the model of CTF-400 simulated by Mercury software (Fig. S3a). Such porous architectures are highly accessible to PPh_3 because the PPh_3 (the longest edge is ~9.403 Å, Fig. S3b) is much smaller than the pore size of CTF-400. In addition, the sample CTF-400 has a high weight ratio of nitrogen (7.57 wt%), which is considered as the ideal precursor to fabricate porous nitrogen-rich carbons via thermal transformation. In order to encapsulate PPh_3 into the porous framework of CTF-400, a facile impregnation method was employed and by adjusting the mass ratio of CTF-400 to PPh_3 in this process, the heteroatom content can be easily tailored.

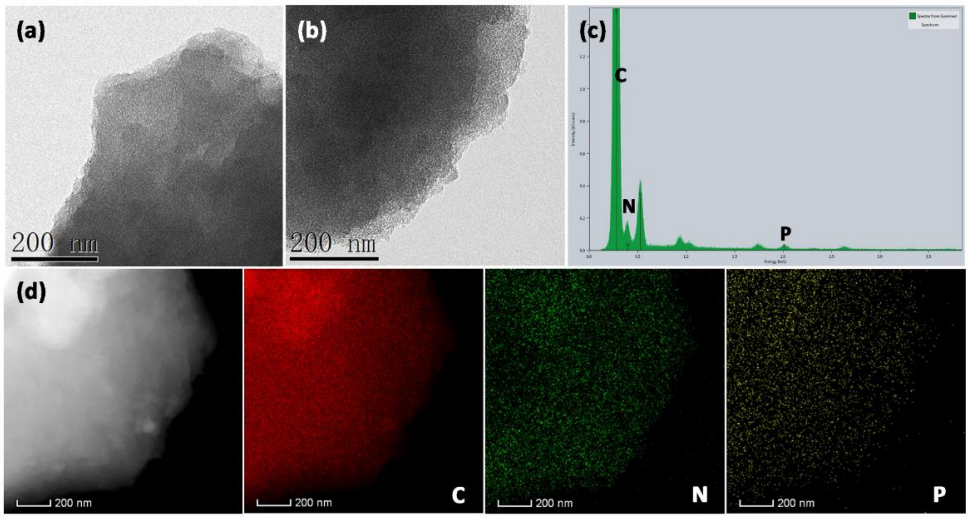

Fig. 2. TEM images of (a) PCTF-1000-5 and (b) CTF-1000; (c) EDX profile of PCTF-1000-5 and (d) the corresponding C, N, and P EDS elemental mappings

The morphology and structure of PCTF-1000-5 were firstly characterized by scanning electron microscopy (SEM). As depicted in Fig. S4, the PCTF-1000-5 presents the block-like morphology with random open pores stacked arbitrarily by the 2D graphene sheets. The transmission electron microscopy (TEM) images (Figs. 2a, b and Fig. S5a) exhibit that the as-prepared PCTF-1000-5 has similar morphology to CTF-1000, suggesting that the highly porous structure was remained after P doping. The energy dispersive X-ray spectroscopy (EDX) (Fig. 2c) manifests the presence of C, N and P elements in PCTF-1000-5, which agrees well with the EA and ICP-AES results (Table S1). The EDS elemental mappings reveal the uniform distribution of these elements within the entire framework (Fig. 2d). The powder X-ray diffraction (PXRD) patterns of all the obtained N,P dual-doped carbons and CTF-1000 (Fig. 3a)

display two broad characteristic peaks at around 25 ° and 44 °, which can be ascribed to the (001) and (101) reflections of graphitic carbon, respectively. The appearance of a weak peak at 44 ° suggested that a higher graphitic degree was obtained in these samples in comparison to precursor CTF-400. The graphitization degrees of all carbon-based materials were further confirmed by Raman spectroscopy. As shown in Fig. 3b, all the samples have typical D bands located at ca. 1355 cm^{-1} and G bands at ca. 1576 cm^{-1}, corresponding to structure defects and the vibration of sp^2-bonded carbon atoms, respectively[32, 40, 54, 55]. Compared with that of CTF-1000, the N,P dual-doped carbons showed larger values of I_D/I_G (Table S2), indicating the presence of more defects in the carbon lattice due to the introduction of P atoms[12, 56]. In addition, a broad weak peak at ca. 2880 cm^{-1} can be observed, suggesting the existence of graphitic layered structures in these samples[57, 58], which is beneficial for the electron transfer to active sites and substrates, thus improving the electrocatalytic activity.

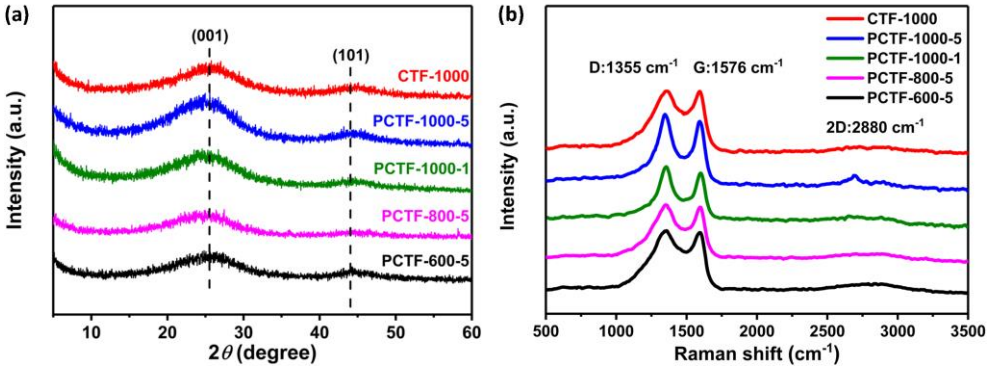

Fig. 3. (a) PXRD patterns and (b) Raman spectra for CTF-1000, PCTF-1000-5, PCTF-1000-1, PCTF-800-5 and PCTF-600-5

To manifest the local chemical environment of all the carbon samples, X-ray photoelectron spectroscopy (XPS) were recorded. The survey spectrum of CTF-1000 shows the presence of C, N and O atoms, while PCTF-1000-5 has a new weak peak positioned at ～133 eV corresponding to the P 2p (Fig. 4a)[33, 38, 45, 56], further confirming that the P species has been successfully introduced into the carbon skeleton. The result matches well with the ICP-AES (Table S1) and EDX results (Figs. 2c, d and Figs. S5b, c). Notably, the O signals in the samples may be originated from physical adsorption of small molecules (e.g., O_2, CO_2 and H_2O) on porous carbons[39]. As shown in Fig. 4b, the high-resolution XPS spectrum for N 1*s* of PCTF-1000-5 can be fitted into four peaks assigned to the pyridinic-N (398.5 eV), pyrrolic-N (399.7 eV), graphitic-N (401.2 eV) and oxidic-N (402.7 eV), respectively[37, 40, 41, 47]. The P 2*p* XPS spectrum reveals three bonding configurations, corresponding to P–C (132.5 eV), P–N (133.7 eV) and P–O (135.0 eV), respectively (Fig. 4c)[40, 45, 56, 59]. The proposed structures of these types of N and P are displayed in Fig. 4d. As comparison, CTF-1000, PCTF-1000-1, PCTF-800-5 and PCTF-600-5 were also characterized by XPS. As depicted in Figs. S6 and S7, the types of N species and the bonding configurations of P element in these samples are similar with those in PCTF-1000-5. The contents of different types of N and P for the samples mentioned above are listed in Tables S3-6 and compared intuitively in Fig. S8. As can be seen from Figs. S8a, b, graphitic-N is the main type N for CTF-1000. Thus, in combining with the ICP-AES and Raman results, it can be concluded that the CTF-1000 retained major sp^2 carbon skeleton. According to previous reports, the C atoms next to pyridinic-N are beneficial for enhancing the CO_2RR activity[52, 55]. Nevertheless, CTF-1000 had the low pyridinic-N amount of 0.03 wt%, while the N,P dual-doped carbon PCTF-800-5-1 exhibited the highest pyridinic-N amount (0.97 wt%), followed by PCTF-1000-5 (0.55 wt%), PCTF-600-5 (0.46 wt%) and PCTF-1000-1 (0.46 wt%) (Table S5). In addition, the P–C bond is regarded to be in favor of CO_2RR in reported P-doped carbons owing to its good CO_2 activation and strong intermediate adsorption[32]. Therefore, the more P–C bonds in N,P dual-doped carbons may also improve the CO_2RR activity. As shown in Table S6, the amounts of P–C bond in PCTF-1000-5, PCTF-1000-1, PCTF-800-5 and PCTF-600-5 are 0.33 wt%, 0.05 wt%, 0.31 wt% and 0.36 wt%, respectively. Here, it is speculated that the N and P owning different electronegativity doped in graphene sheet would activate the adjacent C to P atoms acting as active

sites and the high total amount of pyridinic-N and P–C bond is conducive to electrocatalysis.

In order to determine the porosity and specific surface area of the samples, the nitrogen sorption isotherms were measured at 77 K and the results are shown in Fig. 5a. Compared with mono N-doped CTF-1000, the N,P dual-doped catalysts (PCTF-1000-5, PCTF-1000-1, PCTF-800-5 and PCTF-600-5) showed higher N_2 adsorption capacity. As summarized in Table S7, the BET specific surface areas of PCTF-1000-5, PCTF-800-5 and PCTF-600-5 are 822, 666 and 615 $m^2 \cdot g^{-1}$, respectively, suggesting that the higher carbonization temperature leads to a larger BET specific surface area under the same mass ratio of CTF-400 to PPh_3. The PCTF-1000-5 catalyst also exhibited a larger BET specific surface than that of PCTF-1000-1 (475 $m^2 \cdot g^{-1}$) and CTF-1000 (179 $m^2 \cdot g^{-1}$), which indicated that the large BET specific surface area was related to high N and P doping level at the same carbonization temperature. The pore size distributions calculated by the NL-DFT method (Fig. S9) demonstrated that the pore types of all samples are mainly micropores less than 2 nm in diameter. And the total pore volume of samples displayed a rise with the increased carbonization temperature under the same mass ratio of CTF-400 to PPh_3 or the increased N and P doping level at the same carbonization temperature, which revealed a similar trend to BET specific surface area (Table S7). The high BET surface area and large pore volume could make more active sites highly accessible to substrates, thus improving the energy conversion efficiency. In addition, the highly porous structure is favorable for CO_2 adsorption uptakes, and thereby the adsorption behavior of different samples also revealed the similar regularity to BET specific surface area. It is noteworthy that PCTF-1000-5 with the largest BET surface area exhibited the best CO_2 adsorption capacity of 58 $cm^3 \cdot g^{-1}$ at 298 K (Fig. 5b), which manifested a strong CO_2 affinity by the PCTF-1000-5 that would contribute to improving its CO_2RR activity.

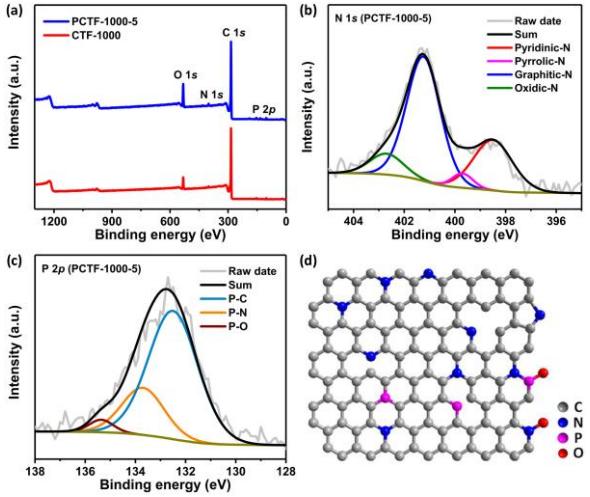

Fig. 4. (a) XPS survey spectra of PCTF-1000-5 and CTF-1000. (b) High-resolution N 1*s* spectrum of PCTF-1000-5. (c) High-resolution P 2*p* spectrum of PCTF-1000-5. (d) Schematic of the proposed structure of N,P dual-doped carbon

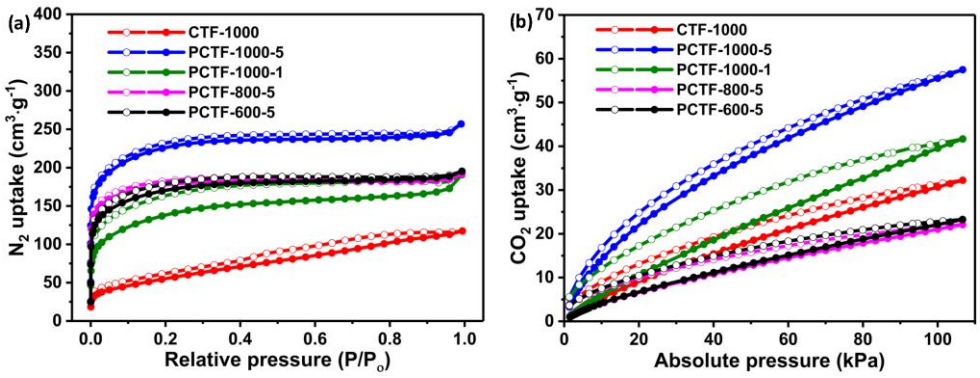

Fig. 5. (a) N_2 adsorption-desorption isotherms and (b) CO_2 adsorption-desorption isotherms of CTF-1000, PCTF-1000-5, PCTF-1000-1, PCTF-800-5 and PCTF-600-5

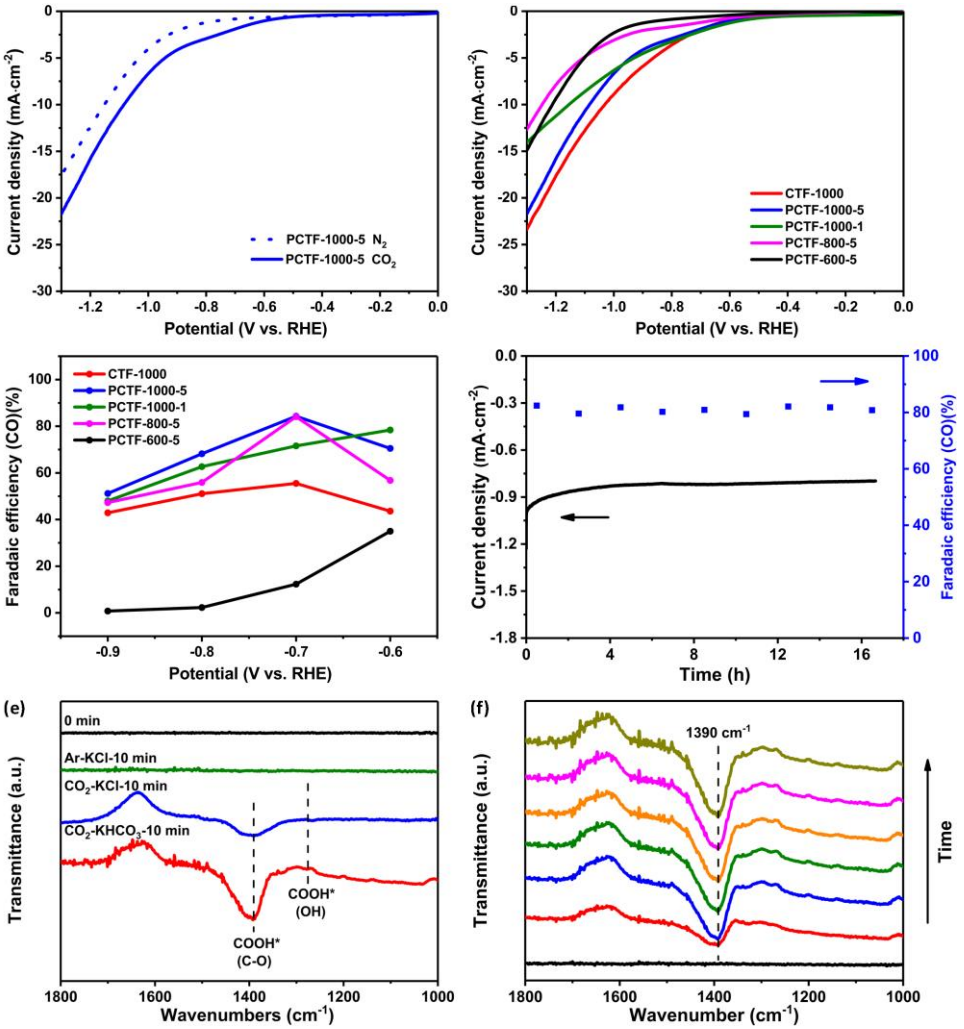

Fig. 6. (a) LSV curves of PCTF-1000-5 in N_2- and CO_2-saturated 0.5 M $KHCO_3$ electrolyte at a scan rate of 10 mV s^{-1}. (b) LSV curves of CTF-1000, PCTF-1000-5, PCTF-1000-1, PCTF-800-5 and PCTF-600-5 in CO_2-saturated 0.5 M $KHCO_3$ electrolyte at a scan rate of 10 mV s^{-1}. (c) FE for CO production of CTF-1000, PCTF-1000-5, PCTF-1000-1, PCTF-800-5 and PCTF-600-5 at different applied potentials. (d) Stability test (FE for CO and total current density) of PCTF-1000-5 at –0.7 V vs. RHE for 16 h. (e) *Operando* ATR-FTIR experiments was taken after 10 min at –0.7 V vs. RHE on the PCTF-1000-5. The green spectrum was taken in 0.1 M KCl saturated with Ar. The blue spectrum was taken in 0.1 M KCl saturated with CO_2. The red spectrum was taken in 0.5 M $KHCO_3$ saturated with CO_2. (f) *Operando* ATR-FTIR of PCTF-1000-5 at –0.7 V vs. RHE in 0.5 M $KHCO_3$ saturated with CO_2

The CO_2RR performances of all the N,P dual-doped carbons and CTF-1000 were conducted in a gas-tight H-type electrochemical cell using an electrolyte of 0.5 M $KHCO_3$. Primarily, the linear sweep voltammetry (LSV) of PCTF-1000-5 was measured between 0 and –1.3 V vs. RHE in both N_2 and CO_2-saturated electrolytes (Fig. 6a). In CO_2-saturated electrolyte, PCTF-1000-5 achieved a more positive onset potential and higher current density than those in N_2-saturated electrolyte, indicating a favorable CO_2 reactivity with the catalyst. As displayed in Fig. 6b, among all the N,P dual-doped samples, PCTF-1000-5 has the most positive onset potential of around –0.48 V vs. RHE and the highest current density of 21.7 mA·cm^{-2} at –1.3 V vs. RHE, strongly indicating that PCTF-1000-5 with the large surface areas, highly porous architectures and synergistic effect of N and P dopants has the best CO_2RR activity. To further determine the selectivity of different catalysts in CO_2RR, the reduction products and corresponding FE at various applied potentials were analyzed. Within the potential ranges from –0.6 to –0.9 V vs. RHE, CO and H_2 were the main gas-phase products detected by gas chromatography (GC), and no liquid-phase product was found in ^{1}H nuclear magnetic resonance (NMR) spectroscopy (Fig. S10). As shown in Figs. 6b, c, CTF-1000 displayed the larger current density and more positive onset potential when compared with N,P dual-doped electrocatalysts, but H_2 was the major product for CTF-1000 during

CO_2RR. The large current density of CTF-1000 might be related to its high graphitization degree indicated by Raman analysis, while the poor CO selectivity is mainly caused by the low pyridinic-N amount in CTF-1000. It can be seen in Fig. 6c that the N,P dual-doped samples PCTF-1000-5, PCTF-800-5 and PCTF-1000-1 exhibited much better CO selectivity than pristine CTF-1000 over the whole applied potential range, which suggested that the doping of P atoms in the N-doped graphitic networks is beneficial for the conversion of CO_2-to-CO. In addition, PCTF-1000-5 achieved higher CO selectivity (84.3%) than PCTF-1000-1 (78.4%), which can be attributed to its higher amount of pyridinic-N (0.55 wt%) and P-C bond (0.33 wt%) than PCTF-1000-1 (0.46 wt% for pyridinic-N; 0.05 wt% for P-C bond). PCTF-800-5 with the higher amount of pyridinic-N (0.97 wt%) and P-C bond (0.31 wt%) than PCTF-1000-1 also gained the higher CO selectivity (84.1%). It should be noted that PCTF-1000-5 with the smaller amount of pyridinic-N and P–C bond than PCTF-800-5 showed higher CO selectivity. This might result from the much higher surface areas of PCTF-1000-5 than PCTF-800-5, which is in favor of the exposure of more active sites and CO_2 adsorption, thus improving the CO yield during CO_2RR. For PCTF-1000-5, it achieved the best FE_{CO} of 84.3% at –0.7 V vs. RHE and gradually decreased with the increase of applied potentials, most likely because the potentials more negative than –0.7 V vs. RHE favored the competitive HER. Significantly, the optimal FE_{CO} of PCTF-1000-5 is superior to most of the previously reported metal-free carbon catalysts (Table S8). It can be also seen in Fig. 6c that PCTF-600-5 showed the worst CO selectivity among all the samples, most likely because the part framework of CTF-400 that is inactive for CO_2RR (Fig. S11) was retained in PCTF-600-5. Long-term stability is another key parameter for a superior electrocatalyst. As shown in Fig. 6d, the electrochemical reduction of CO_2 on PCTF-1000-5 was performed at the applied potential of –0.7 V vs. RHE. The total current density and FE_{CO} have no obvious loss during the entire process of electrolysis for 16 h.

Operando attenuated total reflectance Fourier transform infrared spectroscopy (ATR-FTIR) was employed to explore the possible reaction intermediates during CO_2RR and gain insights into the reaction pathways of CO_2RR over PCTF-1000-5. As shown in Fig. 6e, at an applied potential of –0.7 V vs. RHE, the 1390 cm^{-1} peak associated with the C–O stretch of COOH*[60-62] can be seen clearly in the spectrum obtained in CO_2-saturated 0.5 M $KHCO_3$ and its intensity increased gradually with time and finally reached dynamic balance (Fig. 6f). In addition, a weak peak at 1275 cm^{-1} belonging to the OH-deformation of COOH*[60-62] was also observed. Thus, it is speculated that the formation of *COOH intermediate was the rate-determining step in the conversion of CO_2 to CO for PCTF-1000-5.

3 CONCLUSION

In conclusion, we fabricated a series of N,P dual-doped porous carbons through a one-step carbonization process by using PPh_3@covalent triazine framework composites as precursors. Among all the investigated catalysts, the resulting PCTF-1000-5 achieved the best CO selectivity with 84.3% Faradaic efficiency and favorable stability (over 16 h) for CO_2 reduction, which are superior to the reported N,P dual-doped catalysts in aqueous media. The excellent performance of PCTF-1000-5 can be reasonably attributed to its high specific surface areas, highly porous architectures as well as the synergistic effect between N and P atoms. *Operando* ATR-FTIR demonstrated that the formation of COOH* intermediate was the rate-determining step in CO_2-to-CO conversion. This work will further facilitate the rational design and cost-saved construction of efficient metal-free electrocatalysts for both energy storage and conversions.

REFERENCES

(1) Duan, X.; Xu, J.; Wei, Z.; Ma, J.; Guo, S.; Wang, S.; Liu, H.; Dou, S. Metal-free carbon materials for CO_2 electrochemical reduction. *Adv. Mater.* **2017**, 29, 1701784.

(2) Yi, J. D.; Xie, R.; Xie, Z. L.; Chai, G. L.; Liu, T. F.; Chen, R. P.; Huang, Y. B.; Cao, R. Highly selective CO_2 electroreduction to CH_4 by *in situ* generated Cu_2O single-type sites on a conductive MOF: stabilizing key intermediates with hydrogen bonding. *Angew. Chem. Int. Ed.* **2020**, 59, 23641–23648.

(3) Wu, Q.; Mao, M. J.; Wu, Q. J.; Liang, J.; Huang, Y. B.; Cao, R. Construction of donor-acceptor heterojunctions in covalent organic framework for enhanced CO_2 electroreduction. *Small* **2020**, 2004933.

(4) Zhu, H. J.; Lu, M.; Wang, Y. R.; Yao, S. J.; Zhang, M.; Kan, Y. H.; Liu, J.; Chen, Y.; Li, S. L.; Lan, Y. Q. Efficient electron transmission in covalent organic framework nanosheets for highly active electrocatalytic carbon dioxide reduction. *Nat. Commun.* **2020**, 11, 497.

(5) Ye, K.; Wang, G. X.; Bao, X. H. Electrodeposited Sn-based catalysts for CO_2 electroreduction. *Chin. J. Struct. Chem.* **2020**, 39, 206–213.

(6) Lu, M.; Zhang, M.; Liu, C. G.; Liu, J.; Shang, L. J.; Wang, M.; Chang, J. N.; Li, S. L.; Lan, Y. Q. Stable dioxin-linked metallophthalocyanine covalent organic frameworks (COFs) as photo-coupled electrocatalysts for CO_2 reduction. *Angew. Chem. Int. Ed.* **2021**, DOI:10.1002/anie.202011722.

(7) Huang, Q.; Li, Q.; Liu, J.; Wang, Y. R.; Wang, R.; Dong, L. Z.; Xia, Y. H.; Wang, J. L.; Lan, Y. Q. Disclosing CO_2 activation mechanism by hydroxyl-induced crystalline structure transformation in electrocatalytic process. *Matter* **2019**, 1, 1656–1668.

(8) Hou, S. S.; Xu, Z. T.; Zhang, Y. K.; Xie, K.; Gan, L. Z. Enhanced CO_2 electrolysis with Mn-doped $SrFeO_3$-delta cathode. *Chin. J. Struct. Chem.* **2020**, 39, 1662–1668.

(9) Xu, Z. T.; Xie, K. Enhanced CO_2 electrolysis with metal-oxide interface structures. *Chin. J. Struct. Chem.* **2021**, 40, 31–41.

(10) Nielsen, D. U.; Hu, X. M.; Daasbjerg, K.; Skrydstrup, T. Chemically and electrochemically catalysed conversion of CO_2 to CO with follow-up utilization to value-added chemicals. *Nat. Catal.* **2018**, 1, 244–254.

(11) Sheng, W. C.; Kattel, S.; Yao, S. Y.; Yan, B. H.; Liang, Z. X.; Hawxhurst, C. J.; Wu, Q. Y.; Chen, J. G. G. Electrochemical reduction of CO_2 to synthesis gas with controlled CO/H_2 ratios. *Energy Environ. Sci.* **2017**, 10, 1180–1185.

(12) Wu, J. J.; Yadav, R. M.; Liu, M. J.; Sharma, P. P.; Tiwary, C. S.; Ma, L. L.; Zou, X. L.; Zhou, X. D.; Yakobson, B. I.; Lou, J.; Ajayan, P. M. Achieving highly efficient, selective, and stable CO_2 reduction on nitrogen-doped carbon nanotubes. *Acs Nano* **2015**, 9, 5364–5371.

(13) Long, C.; Li, X.; Guo, J.; Shi, Y. N.; Liu, S. Q.; Tang, Z. Y. Electrochemical reduction of CO_2 over heterogeneous catalysts in aqueous solution: recent progress and perspectives. *Small Methods* **2019**, 3, 1800369.

(14) Zhang, M. D.; Si, D. H.; Yi, J. D.; Zhao, S. S.; Huang, Y. B.; Cao, R. Conductive phthalocyanine-based covalent organic framework for highly efficient electroreduction of carbon dioxide. *Small* **2020**, 16, 2005254.

(15) Mezzavilla, S.; Horch, S.; Stephens, I. E. L.; Seger, B.; Chorkendorff, I. Structure sensitivity in the electrocatalytic reduction of CO_2 with gold catalysts. *Angew. Chem. Int. Ed.* **2019**, 58, 3774–3778.

(16) Li, Y. F.; Chen, C.; Cao, R.; Pan, Z. W.; He, H.; Zhou, K. B. Dual-atom Ag_2/graphene catalyst for efficient electroreduction of CO_2 to CO. *Appl. Catal. B-Environ.* **2020**, 268, 118747.

(17) Gao, D. F.; Zhou, H.; Cai, F.; Wang, J. G.; Wang, G. X.; Bao, X. H. Pd-containing nanostructures for electrochemical CO_2 reduction reaction. *ACS Catal.* **2018**, 8, 1510–1519.

(18) Wang, A.; Li, J.; Zhang, T. Heterogeneous single-atom catalysis. *Nat. Rev. Chem.* **2018**, 2, 65–81.

(19) Yang, H. B.; Hung, S. F.; Liu, S.; Yuan, K. D.; Miao, S.; Zhang, L. P.; Huang, X.; Wang, H. Y.; Cai, W. Z.; Chen, R.; Gao, J. J.; Yang, X. F.; Chen, W.; Huang, Y. Q.; Chen, H. M.; Li, C. M.; Zhang, T.; Liu, B. Atomically dispersed Ni(I) as the active site for electrochemical CO_2 reduction. *Nat. Energy* **2018**, 3, 140–147.

(20) Hou, Y.; Chai, G. L.; Liang, Y. L.; Yi, J. D.; Zhang, T.; Zang, K. T.; Luo, J.; Xu, R.; Lin, H.; Zhang, S. Y.; Wang, H. M.; Huang, Y. B.; Cao, R. Unraveling the reactivity and selectivity of atomically isolated metal-nitrogen sites anchored on porphyrinic triazine frameworks for electroreduction of CO_2. *CCS Chem.* **2019**, 1, 384–395.

(21) Zheng, T. T.; Jiang, K.; Ta, N.; Hu, Y. F.; Zeng, J.; Liu, J. Y.; Wang, H. T. Large-scale and highly selective CO_2 electrocatalytic reduction on nickel single-atom catalyst. *Joule* **2019**, 3, 265–278.

(22) Zhao, C.; Dai, X.; Yao, T.; Chen, W.; Wang, X.; Wang, J.; Yang, J.; Wei, S.; Wu, Y.; Li, Y. Ionic exchange of metal organic frameworks to access single nickel sites for efficient electroreduction of CO_2. *J. Am. Chem. Soc.* **2017**, 139, 8078–8081.

(23) Jiao, L.; Yang, W.; Wan, G.; Zhang, R.; Zheng, X.; Zhou, H.; Yu, S. H.; Jiang, H. L. Single-atom electrocatalysts from multivariate metal-organic frameworks for highly selective reduction of CO_2 at low pressures. *Angew. Chem. Int. Ed.* **2020**, 59, 20589–20595.

(24) Zhang, W. J.; Hu, Y.; Ma, L. B.; Zhu, G. Y.; Wang, Y. R.; Xue, X. L.; Chen, R. P.; Yang, S. Y.; Jin, Z. Progress and perspective of electrocatalytic CO_2 reduction for renewable carbonaceous fuels and chemicals. *Adv. Sci.* **2018**, 5, 1700275.

(25) Zhang, Q. Q.; Guan, J. Q. Single-atom catalysts for electrocatalytic applications. *Adv. Funct. Mater.* **2020**, 30, 2000768.

(26) Pan, Y.; Qian, Y.; Zheng, X.; Chu, S. Q.; Yang, Y.; Ding, C.; Wang, X.; Yu, S. H.; Jiang, H. L. Precise fabrication of single-atom alloy co-catalyst with optimal charge state for enhanced photocatalysis. *Natl. Sci. Rev.* **2021**, 8, nwaa224.

(27) Jiao, L.; Zhang, R.; Wan, G.; Yang, W.; Wan, X.; Zhou, H.; Shui, J.; Yu, S. H.; Jiang, H. L. Nanocasting SiO_2 into metal-organic frameworks

imparts dual protection to high-loading Fe single-atom electrocatalysts. *Nat. Commun.* **2020**, 11, 2831.

(28) Benzigar, M. R.; Talapaneni, S. N.; Joseph, S.; Ramadass, K.; Singh, G.; Scaranto, J.; Ravon, U.; Al-Bahily, K.; Vinu, A. Recent advances in functionalized micro and mesoporous carbon materials: synthesis and applications. *Chem. Soc. Rev.* **2018**, 47, 2680–2721.

(29) Paul, R.; Zhu, L.; Chen, H.; Qu, J.; Dai, L. M. Recent advances in carbon-based metal-free electrocatalysts. *Adv. Mater.* **2019**, 31, 1806403.

(30) Liu, X.; Dai, L. M. Carbon-based metal-free catalysts. *Nat. Rev. Mater.* **2016**, 1, 16064.

(31) You, S. J.; Ma, M.; Wang, W.; Qi, D. P.; Chen, X. D.; Qu, J. H.; Ren, N. Q. 3D Macroporous nitrogen-enriched graphitic carbon scaffold for efficient bioelectricity generation in microbial fuel Cells. *Adv. Energy Mater.* **2017**, 7, 1601364.

(32) Sharma, P. P.; Wu, J.; Yadav, R. M.; Liu, M.; Wright, C. J.; Tiwary, C. S.; Yakobson, B. I.; Lou, J.; Ajayan, P. M.; Zhou, X. D. Nitrogen-doped carbon nanotube arrays for high-efficiency electrochemical reduction of CO_2: on the understanding of defects, defect density, and selectivity. *Angew. Chem. Int. Ed.* **2015**, 54, 13701–13705.

(33) Liu, T.; Ali, S.; Lian, Z.; Si, C.; Su, D. S.; Li, B. Phosphorus-doped onion-like carbon for CO_2 electrochemical reduction: the decisive role of the bonding configuration of phosphorus. *J. Mater. Chem. A* **2018**, 6, 19998–20004.

(34) Xie, J.; Zhao, X.; Wu, M.; Li, Q.; Wang, Y.; Yao, J. Metal-free fluorine-doped carbon electrocatalyst for CO_2 reduction outcompeting hydrogen evolution. *Angew. Chem. Int. Ed.* **2018**, 57, 9640–9644.

(35) Hu, C. G.; Dai, L. M. Doping of carbon materials formetal-free electrocatalysis. *Adv. Mater.* **2019**, 31, 1804672.

(36) Yang, W. G.; Gong, Z. W.; Chen, Y. N.; Chen, R. R.; Meng, D. L.; Cao, M. N. Nitrogen doped carbon as efficient catalyst toward oxygen reduction reaction. *Chin. J. Struct. Chem.* **2020**, 39, 287–293.

(37) Cui, X.; Pan, Z.; Zhang, L.; Peng, H.; Zheng, G. Selective etching of nitrogen-doped carbon by steam for enhanced electrochemical CO_2 reduction. *Adv. Energy Mater.* **2017**, 7, 1701456.

(38) Chen, Y. Z.; Wang, C.; Wu, Z. Y.; Xiong, Y.; Xu, Q.; Yu, S. H.; Jiang, H. L. From bimetallic metal-organic framework to porous carbon: high surface area and multicomponent active dopants for excellent electrocatalysis. *Adv. Mater.* **2015**, 27, 5010–5016.

(39) Zhu, L. W.; Wu, J.; Zhang, Q.; Li, X. K.; Li, Y. M.; Cao, X. B. Chemical-free fabrication of N, P dual-doped honeycomb-like carbon as an efficient electrocatalyst for oxygen reduction. *J. Colloid Interface Sci.* **2018**, 510, 32–38.

(40) Xue, X.; Yang, H.; Yang, T.; Yuan, P.; Li, Q.; Mu, S.; Zheng, X.; Chi, L.; Zhu, J.; Li, Y.; Zhang, J.; Xu, Q. N,P-coordinated fullerene-like carbon nanostructures with dual active centers toward high-efficient multi-functional electrocatalysis for CO_2RR, ORR and Zn-air battery, *J. Mater. Chem. A* **2019**, 7, 15271–15277.

(41) Chen, C.; Sun, X.; Yan, X.; Wu, Y.; Liu, H.; Zhu, Q.; Bediako, B. B. A.; Han, B. Boosting CO_2 electroreduction on N,P-Co-doped carbon aerogels. *Angew. Chem. Int. Ed.* **2020**, 59, 11123–11129.

(42) Kuhn, P.; Antonietti, M.; Thomas, A. Porous, covalent triazine-based frameworks prepared by ionothermal synthesis. *Angew. Chem. Int. Ed.* **2008**, 47, 3450–3453.

(43) Zhao, Y. F.; Yao, K. X.; Teng, B. Y.; Zhang, T.; Han, Y. A perfluorinated covalent triazine-based framework for highly selective and water-tolerant CO_2 capture. *Energy Environ. Sci.* **2013**, 6, 3684–3692.

(44) Puthiaraj, P.; Lee, Y. R.; Zhang, S. Q.; Ahn, W. S. Triazine-based covalent organic polymers: design, synthesis and applications in heterogeneous catalysis. *J. Mater. Chem. A* **2016**, 4, 16288–16311.

(45) Cheng, Z.; Fang, W.; Zhao, T. S.; Fang, S. Q.; Bi, J. H.; Liang, S. J.; Li, L. Y.; Yu, Y.; Wu, L. Efficient visible-light-driven photocatalytic hydrogen evolution on phosphorus-doped covalent triazine-based frameworks. *ACS Appl. Mater. Interfaces* **2018**, 10, 41415–41421.

(46) Hao, L.; Zhang, S. S.; Liu, R. J.; Ning, J.; Zhang, G. J.; Zhi, L. J. Bottom-up construction of triazine-based frameworks as metal-free electrocatalysts for oxygen reduction reaction. *Adv. Mater.* **2015**, 27, 3190–3195.

(47) Wu, J.; Liu, M.; Sharma, P. P.; Yadav, R. M.; Ma, L.; Yang, Y.; Zou, X.; Zhou, X. D.; Vajtai, R.; Yakobson, B. I.; Lou, J.; Ajayan, P. M. Incorporation of nitrogen defects for efficient reduction of CO_2 via two-electron pathway on three-dimensional graphene foam. *Nano Lett.* **2016**, 16, 466–470.

(48) Xu, J.; Kan, Y.; Huang, R.; Zhang, B.; Wang, B.; Wu, K. H.; Lin, Y.; Sun, X.; Li, Q.; Centi, G.; Su, D. Revealing the origin of activity in nitrogen-doped nanocarbons towards electrocatalytic reduction of carbon dioxide. **2016**, 9, 1085–1089.

(49) Wang, R.; Sun, X.; Ould-Chikh, S.; Osadchii, D.; Bai, F.; Kapteijn, F.; Gascon, J. Metal-organic-framework-mediated nitrogen-doped carbon for CO_2 electrochemical reduction. *ACS Appl. Mater. Interfaces* **2018**, 10, 14751–14758.

(50) Lu, X.; Tan, T. H.; Ng, Y. H.; Amal, R. Highly selective and stable reduction of CO_2 to CO by a graphitic carbon nitride/carbon nanotube composite

electrocatalyst. *Chem. Eur. J.* **2016**, 22, 11991–11996.

(51) Zhu, Q.; Ma, J.; Kang, X.; Sun, X.; Hu, J.; Yang, G.; Han, B. Electrochemical reduction of CO_2 to CO using graphene oxide/carbon nanotube electrode in ionic liquid/acetonitrile system. *Sci. China Chem.* **2016**, 59, 551–556.

(52) Li, W.; Seredych, M.; Rodriguez-Castellon, E.; Bandosz, T. J. Metal-free nanoporous carbon as a catalyst for electrochemical reduction of CO_2 to CO and CH_4. *ChemSusChem.* **2016**, 9, 606–616.

(53) Ghausi, M. A.; Xie, J.; Li, Q.; Wang, X.; Yang, R.; Wu, M.; Wang, Y.; Dai, L. CO_2 overall splitting by a bifunctional metal-free electrocatalyst. *Angew. Chem. Int. Ed.* **2018**, 57, 13135–13139.

(54) Wang, Y. S.; Chen, J. X.; Wang, G. X.; Li, Y.; Wen, Z. H. Perfluorinated covalent triazine framework derived hybrids for the highly selective electroconversion of carbon dioxide into methane. *Angew. Chem. Int. Ed.* **2018**, 57, 13120–13124.

(55) Kumar, B.; Asadi, M.; Pisasale, D.; Sinha-Ray, S.; Rosen, B. A.; Haasch, R.; Abiade, J.; Yarin, A. L.; Salehi-Khojin, A. Renewable and metal-free carbon nanofibre catalysts for carbon dioxide reduction. *Nat. Commun.* **2013**, 4, 2819.

(56) Zhang, C.; Mahmood, N.; Yin, H.; Liu, F.; Hou, Y. Synthesis of phosphorus-doped graphene and its multifunctional applications for oxygen reduction reaction and lithium ion batteries. *Adv. Mater.* **2013**, 25, 4932–4937.

(57) Yi, J. D.; Xu, R.; Wu, Q.; Zhang, T.; Zang, K. T.; Luo, J.; Liang, Y. L.; Huang, Y. B.; Cao, R. Atomically dispersed iron-nitrogen active sites within porphyrinic triazine-based frameworks for oxygen reduction reaction in both alkaline and acidic media. *ACS Energy Lett.* **2018**, 3, 883–889.

(58) Chen, Y.; Li, J.; Mei, T.; Hu, X. G.; Liu, D.; Wang, J.; Hao, M.; Li, J.; Wang, J.; Wang, X. Low-temperature and one-pot synthesis of sulfurized graphene nanosheets via *in situ* doping and their superior electrocatalytic activity for oxygen reduction reaction. *J. Mater. Chem. A* **2014**, 2, 20714–20722.

(59) Fang, X. X.; Ma, L. B.; Liang, K.; Zhao, S. J.; Jiang, Y. F.; Ling, C.; Zhao, T.; Cheang, T. Y.; Xu, A. W. The doping of phosphorus atoms into graphitic carbon nitride for highly enhanced photocatalytic hydrogen evolution. *J. Mater. Chem. A* **2019**, 7, 11506–11512.

(60) Deng, W.; Zhang, L.; Li, L.; Chen, S.; Hu, C.; Zhao, Z. J.; Wang, T.; Gong, J. Crucial role of surface hydroxyls on the activity and stability in electrochemical CO_2 reduction. *J. Am. Chem. Soc.* **2019**, 141, 2911–2915.

(61) Firet, N. J.; Smith, W. A. Probing the reaction mechanism of CO_2 electroreduction over Ag films via operando infrared spectroscopy. *ACS Catal.* **2017**, 7, 606–612.

(62) Zhu, S.; Li, T.; Cai, W. B.; Shao, M. CO_2 Electrochemical reduction as probed through infrared spectroscopy. *ACS Energy Lett.* **2019**, 4, 682–689.